DJS Vol. 48 (1) (2024) –pp.172- 185 ISSN: 1012-5965

Delta Journal of Science
Available online at
https://djs.journals.ekb.eg/

Research Article

GEOLOGY

Lithological, structural and hydrothermal alteration mapping utilizing remote sensing datasets: a case study of Ras Abdah- Abu Hadedah area, Northeastern Desert, Egypt

Mahmoud H. Ashmawy [1], Gehad M. Saleh[2], Ibrahim A. Salem[1], Samia G. El-Sharkawy[1*]

[1] Department of Geology, Faculty of Science, Tanta University, Egypt
[2] Nuclear Materials Authority, P.O. Box 530, El Maadi, Cairo, Egypt

[*]**Corresponding author:** Samia G. El Sharkawy **email:** *samia_51218_pg@science.tanta.edu.eg*
samiaelsharkawy1@gmail.com

Received: 20 /3/2024 **Accepted:** 15/4/ 2024

KEY WORDS

Remote sensing, GIS, structural, mapping, lithology, Ras Abdah- Abu Hadedah.

ABSTRACT

Remote sensing datasets have offered amazing breakthroughs in mapping rock units, structural components, and hydrothermal alteration zones. The main objective of this study is to distinguish the lithological elements of Ras Abdah Abu-Hadedah area, Northeastern Desert (NED), Egypt. This study used a multispectral dataset from Landsat-8. Image processing technologies include False Colour Combination (FCC) and Band Ratio (BR) were applied for lithological and alteration mapping. Lineament extraction is done using PCI Geomatica's commonly used LINE module. In addition, the correlation between hydrothermally-altered zones and structural characteristics highlights the need for additional investigation of ore deposits in the research region. These lineaments features are extracted using a panchromatic 15m pixel band. An image processing results provided updated geologic map to the study area. The dominated structural trends are presented in the area by NW-SE and NE-SW trends. This also demonstrates the effectiveness of the data and methods used.

Introduction

Geological mapping is essential for various fields and applications, including mineral exploration, landslides, mining, geomorphology, and flash floods. Remote sensing datasets provide a cost-effective and time-saving alternative to traditional field mapping methods, particularly for inaccessible terrain **(Gad and Kusky, 2006; Pour et al., 2019)**. Landsat data is frequently applied to ide ntify geological units, lineaments, and hy drothermal alteration **(Amer et al., 2012; Pour and Hashim, 2014; Noori et al., 2019)** Landsat data is still employed in many applications, particularly in the latest series (Landsat-8 OLI/TIRS as a result of advanced image processing techniques that can improve specific targets. Landsat-8 has improved spectral properties compared to earlier missions **(Rajendran and Nasir, 2014; van der Werff and van der Meer, 2016and Abd El-Wahed et al., 2019).** This study used Landsat-8 Operational Land Imager (OLI) to identify lithological contacts, structural features, and hydrothermal alteration zones, which might indicate metallogenic sites in the studied area. Landsat-8 data cannot correctly distinguish particular alteration minerals, but can point to the presence of clay minerals, sulphides, iron oxides, carbonate, hydroxyl-bearing, and silicates.

The well-known Gram-Schmidt spectral sharpening method is applied to increase the spatial resolution of multispectral imagery to panchromatic precision (15 m) while keeping the spectral data. This might enhance the visualization of the rock units in the research region to the scale improvement from 30 m to 15 m. In this study, the best RGB combinations for lithological discrimination will be selected. False color composite (FCC), band ratios (BRs) and supervised classification will be used based on the spectrum properties of the bands used, to enhance lithological units and two forms of hydrothermal alteration (ferrugination and OH-bearing minerals) in the area under investigation. Moreover, the study will evaluate the ability of Landsat VNIR and SWIR bands to extract linear characteristics to the efficiency of panchromatic bands.

Geologic Setting

Ras Abdah- Abu Hadedah encompasses part of the Arabian Nubian Shield (ANS). It is located in the North of the Egyptian Eastern Desert and lies between 26o 42' 54", 26o 45' 36" N and longitudes 33o 44' 06", 33o 47' 42" E, where wadi Ras Abdah is located on approximately 20 Km away

southwestern Safaga city as shown in Figure 1. The Precambrian rocks in the study area are arranged chronologically from the oldest to the youngest as follows; metagabbros, metasediments, amphibolites, syn-orogenic granites (older granites-granodiorites), younger gabbros, post-orogenic granites (syenogranites and alkali feldspar granites), post granitic dykes and veins.

Materials and Methods

Landsat-8 is an appealing option among researchers due to its extensive coverage (185 x 180 km), affordable cost, and a noticeable enhancement to the spectral and radiometric resolution (16 bits) compared to previous Landsat sensors **(Roy et al., 2014**). In this study, the thematic mapping was carried out using software (ENVI 5.2 and ArcGIS 10.5). The data was obtained by Landsat-8 freely from USGS Earth Explorer website (http://earthexplorer.usgs.gov) which was obtained on March 18, 2018 (18-3-2018) and includes eleven bands on a cloud-free day. The Landsat-8 mission uses two sensors, OLI (Operational Land Imager) and TIRS (Thermal Infrared Sensor), to collect spectral data in the VNIR, SWIR, and TIR areas **(Rajan Girija and Mayappan, 2019).**

Table (1) shows that OLI data are captured in nine spectral bands, but TIRS data only provide information in two. This research excludes TIRS data. The spectral bands that were utilized are georeferenced to WGS-84, UTM zone 36 N, and atmospherically corrected using the Fast Line-of-Sight Atmospheric Analysis of Spectral Hypercubes (FLAASH) preprocessing procedure in the Environment for Visualizing Images (ENVI) software version 5.2. The best techniques that used for identifying rock units, in the study area, are false color composites (FCCs), band ratios (BRCs) and supervised classification. The results are then pan-sharpened with HSV and shown as FCCs in RGB order. BR is a popular technique for categorizing rock units, identifying hydrothermal alteration, and mineral prospecting. The term "BR" refers to the partition of digital digits (DNs) between two sensor bands. Every kind is subsequently distinguished and mapped using Maximum Likelihood classifier. Definite BRs and FCCs are assigned to detect ferrugination and OH-bearing hydrothermal alterations based on their spectral properties and alteration type. The PCI Geomatica software's supported with LINE module method is used for structural mapping purposes. This method detects edges and creates lines by connecting them **(Koike et al., 1995; Adiri et al., 2017; Masoud and**

Koike, 2017; Shebl and Csámer, 2021b). A detailed lineament study was conducted by examining all VNIR and SWIR bands.

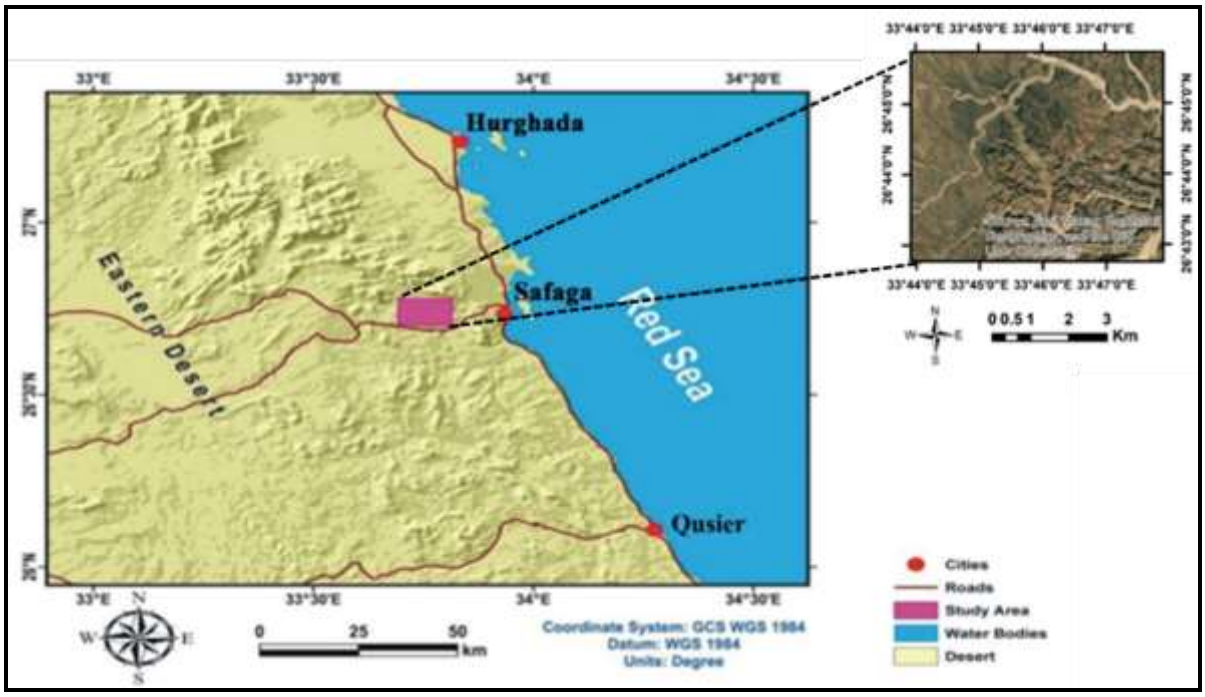

Fig. (1): Location of Ras Abdah- Abu Hadedah area, NED, Egypt.

Table (1): Characteristics of Landsat-8 OLI data

Bands	Central Wave length (mm)	Spatial Resolution (m)
1	0.442	30
2	0.483	30
3	0.561	30
4	0.654	30
5	0.864	30
6	1.609	30
7	2.203	30
8	0.598	15
9	1.373	30
10	10.90	100
11	12.00	100

Results and Discussion

Lithological and hydrothermal alteration mapping

Color composites images

The bands selection should be based mainly on the spectral contrast of the material relative to their surroundings **(Thurmond et al., 2006)**. The features which have specific reflectance characteristics are mainly affected the spectral ratio. True color images (TCC) bands 4, 3 and 2 in RGB for Landsat-8 (Figure 2a), was generated for Ras Abdah-Abu Hadedah area, which are showing a quiet clear lithologic discrimination.

Different false color composites (FCCs) were tested and chosen to get the best vision to discriminate and identify different types of rocks (Table 2). Some of them were applied on Landsat-8 for the study area, which give a reliable and reasonable lithologic discrimination **(Dev Acharya et al., 2015)**. The best results are given in Fig. (2b and 2c) The best representable results are FCC of bands 753 in RGB (Fig. 2b) and FCC of bands 742 in RGB (Fig. 2c).

Table (2): Suggested FCCs applied on Landsat-8 data (some of them used in the present study) as suggested by previous studies

No.	Suggested FCC in RGB	Sensor used	Authors
1	764-763-762-761-754-753-752-751	Landsat OLI	**(Dev Acharya et al., 2015)**
2	742	Landsat OLI	**(Kalelioğ lu et al., 2009)**
3	753, 267, 287, 237	Landsat OLI	**(Saadi and Watanabe, 2009)**

In Figure (2a, b), the yellowish-brown color represents the presence of quartz and feldspars of granites which occupy almost 75% of the whole rock composition. FCC of bands 753 (Fig. 2b) shows syenogranites as dark reddish-brown color as two parallel arrows shaped like, while the background represents synorogenic granites, which appear in a yellowish-brown color. In addition, post-orogenic granites in the northern and southern edge of the study area are masked by a moderate reddish-brown degree. This color graduation may be due to the variation of quartz percentage in synorogenic and post-orogenic granites which affects the reflectance degree.

Band ratioing composites (BRC)

The band ratio is regarded an efficient tool in geological mapping **(Kusky and Ramadan, 2002; Aboelkhair et al., 2010; Emam et al., 2016; Ge et al., 2018)**. Different band ratios were created. Three of them display greater lithological discrimination and structural enhancement. These combinations are (5/1, 4/2, 5/6 in RGB), (6/7, 4/2, 5/4 in RGB) and (6/5, 6/2, 6/7 in RGB).

The band ratioing composite of (5/1, 4/2, 5/6) in RGB, the dyke swarms display in light blue color, syenogranites appear in brownish yellow color, synorogenic granites are coated in greenish yellow color, post-orogenic granites are filmed by a

yellow color, amphibolites are masked by greyish black color and bright blue color manifests the younger gabbros (Fig. 2d). On the other hand, in the band ratioing composite of (6/7, 4/2, 5/4) in RGB, the dyke swarms are visible in light blue color, syenogranites appear in light reddish with white tent, synorogenic granites display in aqua bluish color, post-orogenic granites are represented by dark bluish green color, purple color demonstrates the syenogranites, and reddish color pronounces the younger gabbroic rocks (Fig. 2e). Further, in the band ratioing composite of (6/5, 6/2, 6/7) in RGB, the dyke swarms display in light bluish color, syenogranites appear in a light pink color, synorogenic granites are revealed in a brownish green color, post-orogenic granites are masked by light green with white tint, amphibolites exhibit orange color, and dark blue color overlies the younger gabbroic rocks (Fig. 2f).

Image classification

Classification is a technique that applies categorization of a wide range of variant pixel groups depending on spectral character. Simply, classification can be defined as the process which includes the categorization of the pixel groups of the same spectral characterization and considered to belong to the same class that can be characterized and assigned a significant individual color **(Kamel et al., 2016).**

Supervised classification was defined as the process in which quantitative analysis of remote sensing data is significantly used depending mainly on using a convenient algorithm to label the pixels in an image as representing specific land cover types or classes **(Richards, 2013)**. Different algorithms are used to perform this technique. The chosen algorithms for this classification contain maximum tendency classifier and support vector machine as they quantitatively assess both the deviation and coherence of the category spectral characteristics patterns when labeling an unidentified pixel. These algorithms depend upon training areas to be labeled for every class. Regions of Interest (ROI) (a function in ENVI software) form these training areas and have a noticeable abundance of input from the image analysis and knowledge of the types of land cover that are found in Ras Abdah-Abu Hadedah area. This information is attainable from the available previous maps and from the achievable field works where various surface classes are confirmed and their geographical positions can be determined.

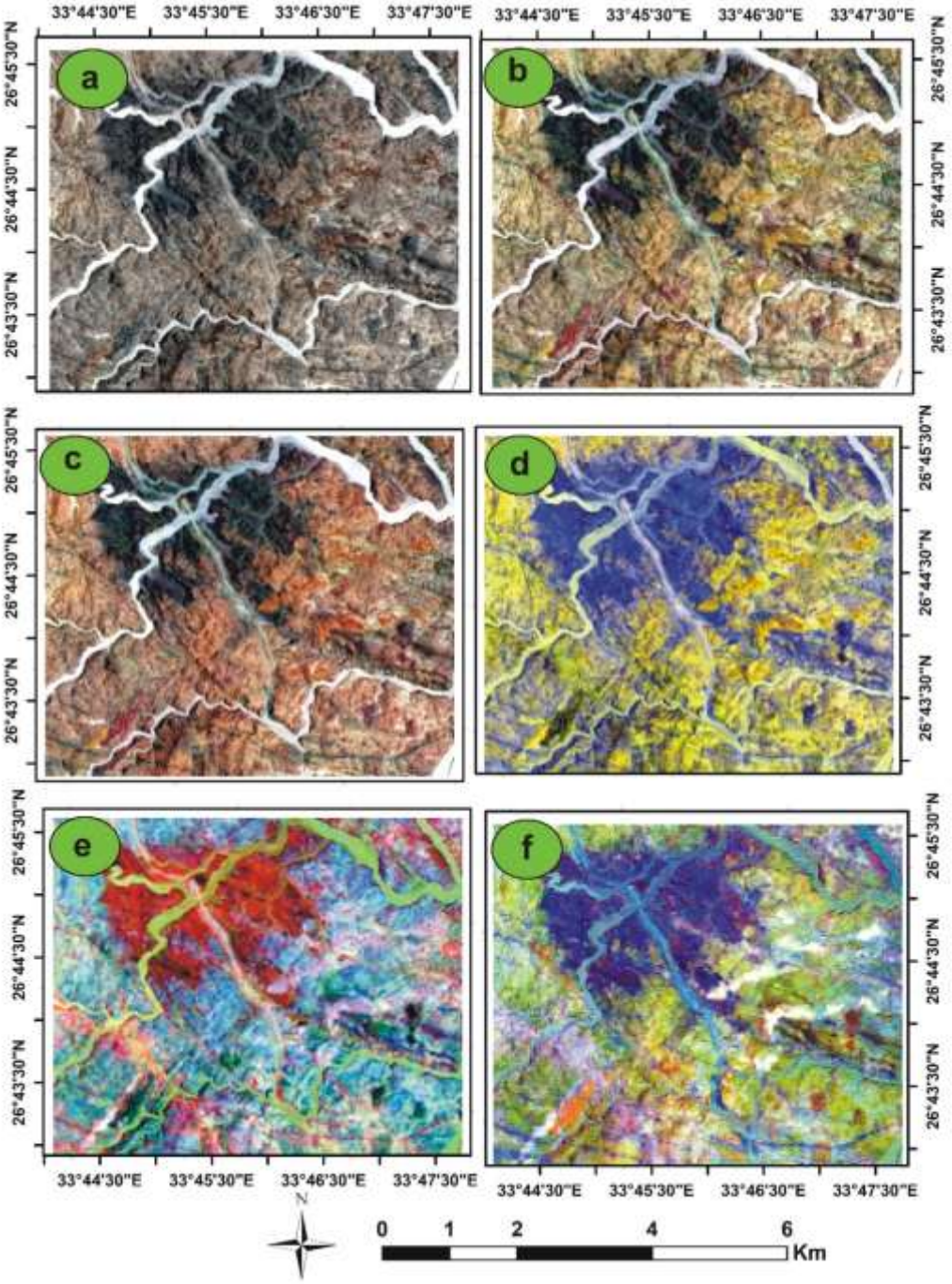

Fig. (2): (a) TCC of RGB 432; (**b)** FCC of RGB 753; (**c)** FCC of RGB 742; **(d)** BRCs of RGB 5/1, 4/2, 5/6 of Landsat-8 of the studied area; **(e)** BRCs of 6/7, 4/2, 5/4 of Landsat-8 of the studied area; **(e)** BRCs of RGB 6/5, 6/2, 6/7 of Landsat-8 of the studied area.

The resultant supervised classification (Maximum Likelihood Classifier) can discriminate between the different rocks from oldest to youngest; (1) Metagabbros, (2) Metasediments, (3) Amphibolite, (4) Syn-orogenic granites (Older granites-granodiorites), (5) Younger gabbro,

(6) post-orogenic granites which classified into Mineralized granites (Syenogranites) and (7) Alkali feldspar granites, (8) Alluvial deposits and mapped in (Fig. 3a,b). In regarding to detect the mineralization zones in the study area. The grey scale band ratio 6/5 shows the ferrugination in bright pixels which enhanced with dark green color where the band ratio 6/7 detected the OH-bearing hydrothermal alteration which enhanced by blue pixels (Fig. 4a). There is a specific term that is used to express the degree of "correctness" of a map or classification in thematic mapping based on remote sensing data, called accuracy **(Foody, 2002)**. The confusion matrix (also referred to as error matrix) is currently at the center of the accuracy assessment literature (Foody, 2002). The accuracy of the classified map resulting from Maximum Likelihood Classifier (Fig. 3a) was estimated with an overall accuracy of 91.39% and a Kappa coefficient of 0.8997.

Structural mapping and Results Integration

The PCI Geomatica software lineament extraction algorithm includes edge detection, thresholding, and curve extraction steps **(Aluko and Igwe, 2018)**. These steps were carried over two shaded relief images under the parameters listed in Table (3). The directional analysis of the automatically extracted lineament maps (Fig. 4b and4c and rose diagram Fig. 5) explained that the most common directions are NW to WNW, ENE, NNW, E-W, N-S, and NNE. This result is closely matched with previously mentioned lineament maps based on detailed structural fieldwork.

This reflects the effectiveness of Landsat-8 data and derived hill shades in the lineament extraction process. Faulting plays an important role in facilitating the alteration processes through the circulation of both hydrothermal solutions and/or meteoric water causing enrichments in large ion lithophile elements like uranium and thorium. This explains the close relationship between the lineament density and the presence of radioactive potentialities related to alteration. A lineament density map was created to display highly dissected areas and their spatial relationship to hydrothermally altered zones. The studied area may include structurally regulated mineral resources, as most alteration zones are found in medium to high-density locations. These findings are highlighted by their proximity to split and altered zones.

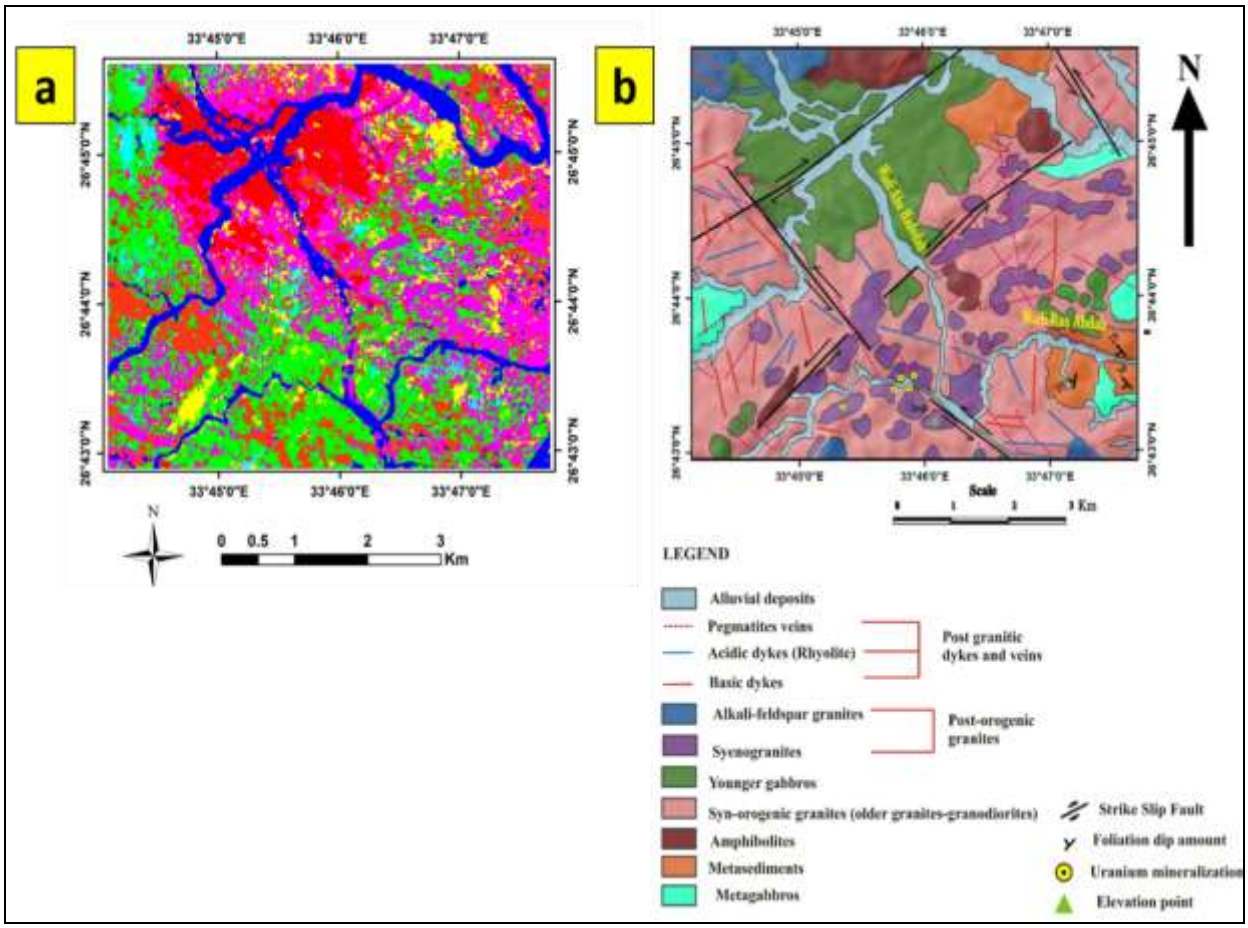

Fig. (3): (a) Maximum Likelihood classification image **(b)** The updated detailed geologic map of Wadi Ras Abdah-Abu Hadedah area, NED, Egypt, based on remote sensing interpretation and field work verification

Table (3): Lineament's extraction parameters of PCI line algorithm.

Parameter	Value
Filter Radius (Pixels)	**10**
Edge Gradient Threshold	**255**
Curve Length Threshold (Pixels)	**25**
Line Fitting Error Threshold (Pixels)	**3**
Angular Difference Threshold (Degrees)	**30**
Linking Distance Threshold (Pixels)	**20**

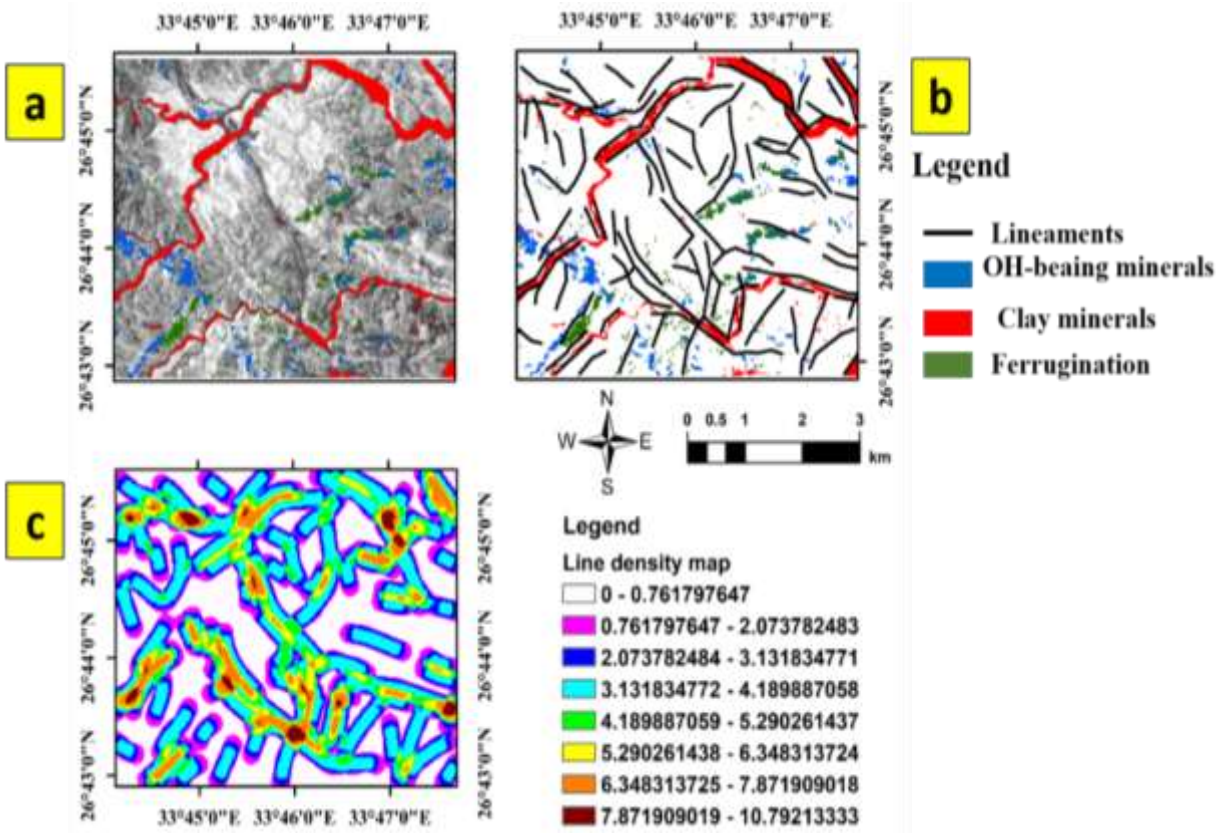

Fig.(4): Hydrothermal alteration zones mapping **(a)** The rich areas with clay minerals are enhanced by red color, ferrugination by green color and the OH-bearing hydrothermal alteration by blue color **(b)** the extracted lineament map; **(c)** Lineaments density map (NO/Km) of Wadi Ras Abdah-Abu Hadedah area, NED, Egypt

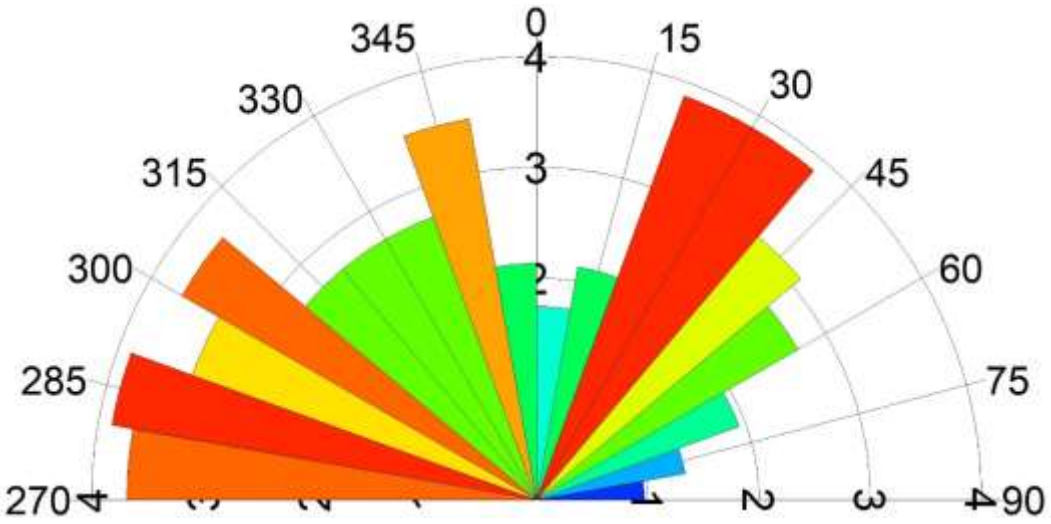

Fig. (5): Rose diagram showing the most common lineaments trends detected in the studied area

Conclusions

The best-obtained results are FCCs of RGB (753and 742) and BRCs of RGB (5/1, 4/2, 5/6); (6/7, 4/2, 5/4); (6/5, 6/2, 6/7) of Landsat-8 of the studied area FCC, BRC, and the resultant supervised classification (Maximum Likelihood Classifier) give the best results and in turn final geologic map.

The results of the present study can be summarized in the following points:

1- Remote sensing datasets quickly execute geological and structural mapping of complicated terrains, and their findings are relatively comparable to costly field mapping approaches.

2- Using a combination of visible, NIR, and SWIR bands is frequently suggested to enhance rock units in study area.

3- Utilizing band ratio technique proves efficiency in identifying rocks and alteration zones based on the utilized data properties.

4- The process of Cross-linking of structural, lithological, and hydrothermal alteration data is a cost-effective and efficient strategy for mineral discovery.

References

Abd El-Wahed, M., Kamh, S., Ashmawy, M., and Shebl, A. (2019). Transpressive Structures in the Ghadir Shear Belt, Eastern Desert, Egypt: Evidence for Partitioning of Oblique Convergence in the Arabian-Nubian Shield during Gondwana Agglutination. *ACTA GEOL SIN-ENGL.*, 93(6): 1614–1646. https://doi.org/10.1111/1755-6724.13882

Aboelkhair, H., Ninomiya, Y., Watanabe, Y., and Sato, I. (2010). Processing and interpretation of ASTER TIR data for mapping of rare-metal-enriched albite granitoids in the Central Eastern Desert of Egypt. *J. Afr. Earth. Sci.*, *58*(1): 141–151. https://doi.org/10.1016/J.JAFREARSCI.2010.01.007

Adiri, Z., El Harti, A., Jellouli, A., Lhissou, R., Maacha, L., Azmi, M., Zouhair, M., and Bachaoui, E. M. (2017). Comparison of Landsat-8, ASTER and Sentinel 1 satellite remote sensing data in automatic lineaments extraction: A case study of Sidi Flah-Bouskour inlier, Moroccan Anti Atlas. *ASR.*, 60(11): 2355–2367. https://doi.org/10.1016/J.ASR.2017.09.006

Aluko, O. E., and Igwe, O. (2018). Automated Geological lineaments mapping for groundwater exploration in the basement complex terrain of Akoko-Edo area, Edo-State Nigeria using remote sensing techniques. *Model. Earth Syst. Environ.*, *4*(4): 1527–1536. https://doi.org/10.1007/S40808-018-0511-4/METRICS

Amer, R., Kusky, T., and El Mezayen, A. (2012). Remote sensing detection of gold related alteration zones in Um Rus area, Central Eastern Desert of Egypt. *ASR.*, 49(1): 121–134. https://doi.org/10.1016/J.ASR.2011.09.024

Dev Acharya, T., Yang, I., and Student, G. (2015). Exploring Landsat 8. *Int. J. of IT, Eng. App. Sci. Res.*, *4*(4): 2319–

4413. http://earthobservatory.nasa.gov/IOTD/

Emam, A., Zoheir, B., and Johnson, P. (2016). ASTER-based mapping of ophiolitic rocks: examples from the Allaqi–Heiani suture, SE Egypt. *Int. Geol. Rev..*, 58(5): 525–539. https://doi.org/10.1080/00206814.2015.1094382

Foody, G. M. (2002). Status of land cover classification accuracy assessment. *RSE.*, 80(1): 185–201. https://doi.org/10.1016/S0034-4257(01)00295-4

Gad, S., and Kusky, T. (2006). Lithological mapping in the Eastern Desert of Egypt, the Barramiya area, using Landsat thematic mapper (TM). *J. Afr. Earth. Sci.*, 44(2): 196–202. https://doi.org/10.1016/J.JAFREARSCI.2005.10.014

Ge, W., Cheng, Q., Jing, L., Armenakis, C., and Ding, H. (2018). Lithological discrimination using ASTER and Sentinel-2A in the Shibanjing ophiolite complex of Beishan orogenic in Inner Mongolia, China. *ASR.*, 62(7): 1702–1716. https://doi.org/10.1016/J.ASR.2018.06.036

J Thurmond, T Loseth, J Rivenaes, O Martinsen, X Xu, C Aiken, and T Nilsen. (2006). Using outcrop data in the 21st Century–New methods and applications, with example from the Ainsa Turbidite System, Ainsa, Spain. *Deep-Water Outcrops of the World Atlas: AAPG., Sp. Pub., CD-ROM*.

Kalelioğ lu, Ö., Zorlu, K., Kurt, M. A., Gül, M., and Güler, C. (2009). Delineating compositionally different dykes in the Ulukışla basin (Central Anatolia, Turkey) using computer-enhanced multi-spectral remote sensing data. *Int. J. Remote Sens. 30*(11): 2997–3011. https://doi.org/10.1080/01431160802558683

Kamel, M., Youssef, M., Hassan, M., and Bagash, F. (2016). Utilization of ETM+ Landsat data in geologic mapping of wadi Ghadir-Gabal Zabara area, Central Eastern Desert, Egypt. *Egypt. J. Remote Sens. Space Sci.*, 19(2): 343–360. https://doi.org/10.1016/J.EJRS.2016.06.003.

Koike, K., Nagano, S., and Ohmi, M. (1995). Lineament analysis of satellite images using a Segment Tracing Algorithm (STA). *Comput. and Geosci.*, 21(9), 1091–1104. https://doi.org/10.1016/0098-3004(95)00042-7

Kusky, T. M., and Ramadan, T. M. (2002). Structural controls on Neoproterozoic mineralization in the South Eastern Desert, Egypt: an integrated field, Landsat TM, and SIR-C/X SAR approach. *J. Afr. Earth Sci.*, 35(1), 107–121. https://doi.org/10.1016/S0899-5362(02)00029-5

Masoud, A., and Koike, K. (2017). Applicability of computer-aided comprehensive tool (LINDA: Lineament Detection and Analysis) and shaded digital elevation model for characterizing and interpreting morphotectonic features from lineaments. *Comput.* and *Geosci.*, 106: 89–100. https://doi.org/10.1016/J.CAGEO.2017.06.006

Noori, L., Pour, A. B., Askari, G., Taghipour, N., Pradhan, B., Lee, C. W., and Honarmand, M. (2019). Comparison of Different Algorithms to Map Hydrothermal Alteration Zones Using ASTER Remote Sensing Data

for Polymetallic Vein-Type Ore Exploration: Toroud–Chahshirin Magmatic Belt (TCMB), North Iran. *Remote Sens.*, 11(5): 495. https://doi.org/10.3390/RS11050495

Pour, A. B., and Hashim, M. (2014). ASTER, ALI and Hyperion sensors data for lithological mapping and ore minerals exploration. *Springerplus*, 3(1): 1–19. https://doi.org/10.1186/2193-1801-3-130/TABLES/3

Pour, A. B., Hashim, M., Hong, J. K., and Park, Y. (2019). Lithological and alteration mineral mapping in poorly exposed lithologies using Landsat-8 and ASTER satellite data: North-eastern Graham Land, Antarctic Peninsula. *Ore Geol. Rev.*, 108: 112–133. https://doi.org/10.1016/J.OREGEOREV.2017.07.018

Rajan Girija, R., and Mayappan, S. (2019). Mapping of mineral resources and lithological units: a review of remote sensing techniques. *Int. J. Image Data Fusion*, 10(2), 79–106. https://doi.org/10.1080/19479832.2019.1589585

Rajendran, S., and Nasir, S. (2014). Hydrothermal altered serpentinized zone and a study of Ni-magnesioferrite–magnetite-awaruite occurrences in Wadi Hibi, Northern Oman Mountain: Discrimination through ASTER mapping. *Ore Geol. Rev.*, 62: 211–226. https://doi.org/10.1016/J.OREGEOREV.2014.03.016

Richards, J. A. (2013). Remote sensing digital image analysis: An introduction. *Remote Sensing Digital Image Analysis: An introduction*, *9783642300622*, 1–494. https://doi.org/10.1007/978-3-642-30062-2/COVER

Roy, D. P., Wulder, M. A., Loveland, T. R., C.E., W., Allen, R. G., Anderson, M. C., Helder, D., Irons, J. R., Johnson, D. M., Kennedy, R., Scambos, T. A., Schaaf, C. B., Schott, J. R., Sheng, Y., Vermote, E. F., Belward, A. S., Bindschadler, R., Cohen, W. B., Gao, F., … Zhu, Z. (2014). Landsat-8: Science and product vision for terrestrial global change research. *RSE.*, 145: 154–172. https://doi.org/10.1016/J.RSE.2014.02.001

Saadi, N. M., and Watanabe, K. (2009). Assessing image processing techniques for geological mapping: a case study in Eljufra, Libya. *Geocarto Int.*, *24*(3): 241–253. https://doi.org/10.1080/10106040802556199

Shebl, A., and Csámer, Á. (2021b). Reappraisal of DEMs, Radar and optical datasets in lineaments extraction with emphasis on the spatial context. *Remote Sens. Appl. Soc. Environ.*, *24*, 100617. https://doi.org/10.1016/J.RSASE.2021.100617

van der Werff, H., and van der Meer, F. (2016). Sentinel-2A MSI and Landsat 8 OLI Provide Data Continuity for Geological Remote Sensing. *Remote Sens.*, *8*(11): 883. https://doi.org/10.3390/RS8110883

التخريط الليثولوجي والتركيبي ونطاقات التحلل الحرمائي باستخدام بيانات الاستشعار عن بعد: دراسة حالة لمنطقة رأس عبده- ابوحديدة شمال الصحراء الشرقية – مصر.

أ.د. محمود حسين العشماوي[١] ، أ.د. جهاد محمد صالح[٢] ، أ.د. ابراهيم عبد الناجي سالم[١] ، سامية جمال الشرقاوي[١*]

١ قسم الجيولوجيا، كلية العلوم، جامعة طنطا

[٢] هيئة المواد النووية ص.ب. ٥٣٠، المعادي ، القاهرة

ان الاستشعار من بعد قد أحدث تطورا مذهلا في شتى المجالات العلمية ومن أحدث التطبيقات العلمية الجيولوجية التي لفتت الأنظار لمدى أهميته هو استخدامه في تنفيذ الخرائط الجيولوجية المحتلفة والاستكشافات المعدنية ، في هذه الدراسة تم استخدام تقنيات مختلفة من الاستشعار من بعد لأجل الوصول لأفضل ناتج للخريطة لهذه المنطقة ، ومن التقنيات المستخدمة (FCC) و BRC و التصنيف الخاضع للاشراف باستخدام الأكثر تشابها. و أفضل النتائج التي تم الحصول عليها من تطبيق (FCC) الخاصة بـ هي RGB (٧٥٣ و ٧٤٢) و BRCs بـ (٥/١، ٢/٤، ٦/٥)؛ (٧/٦، ٢/٤، ٤/٥)؛ (٥/٦، ٢/٦، ٧/٦) للقمر لاندسات٨ لمنطقة الدراسةFCC ، BRC والتصنيف الخاضع للإشراف Maximum) محتمل الاحتمالية (يعطي أفضل النتائج وبالتالي خريطة جيولوجية نهائية. ويمكن تلخيص نتائج الدراسة الحالية في النقاط التالية:

١) تقوم مجموعات بيانات الاستشعار عن بعد بتنفيذ الخرائط الجيولوجية والهيكلية للتضاريس المعقدة بسرعة، وتكون نتائجها قابلة للمقارنة نسبيًا مع طرق رسم الخرائط الميدانية المكلفة.

٢) يقترح بشكل متكرر استخدام مجموعة من النطاقات المرئية و NIR و SWIR لتعزيز الوحدات الصخرية في منطقة الدراسة.

٣) استخدام تقنية نسبة النطاق أثبت كفاءته في تحديد الصخور ومناطق التغير اعتماداً على خصائص البيانات المستخدمة.

٤) تعد عملية الربط المتبادل لبيانات التغيير الهيكلي والصخري والحراري المائي بمثابة استراتيجية فعالة من حيث التكلفة وفعالة لاكتشاف المعادن.